In Situ and Online Monitoring Polymerization-Induced Micellization

Wenxi Ji, Jingjing Yan, Erqiang Chen,* Zichen Li,* and Dehai Liang*

Beijing National Laboratory for Molecular Sciences, Department of Polymer Science and Engineering and the Key Laboratory of Polymer Chemistry and Physics of the Ministry of Education, College of Chemistry and Molecular Engineering, Peking University, Beijing 100871, China

Received March 10, 2008; Revised Manuscript Received April 19, 2008

ABSTRACT: The polymerization-induced micellization of poly(ethylene oxide)-*b*-poly(styrene-*alt*-maleic anhydride) (PEO-*b*-P(S-*alt*-MAn)) in $CHCl_3$ was monitored in situ by laser light scattering. Reversible addition−fragmentation chain transfer (RAFT) polymerization was used to grow the P(S-*alt*-MAn) block onto the PEO macromolecular chain transfer agents (macro-CTAs) at 55 °C. The whole process underwent three stages over time: the induction period, the formation of loose aggregates, and the formation of micelles. The polymerization process and the micellization process were affected mutually: the increase in the degree of polymerization induced the micellization of PEO-*b*-P(S-*alt*-MAn); meanwhile, the formation of core−shell micelles retarded the polymerization rate. At higher polymer concentrations, the mutual effect was even stronger, where smaller size micelles with higher density were obtained.

Introduction

The self-assembly of block copolymers has been studied extensively by both theoretical modelings[1–4] and experimental measurements.[2–10] The well-defined aggregates formed by block copolymers have been found practically or potentially applicable in the fields of drug and gene delivery,[11,12] nanocomposites,[13] lithography,[14,15] etc. Usually, the preparation of the fine structures via self-assembly is difficult to control, is time-consuming, and involves multiple steps.

Under certain polymerization conditions, diblock copolymers will form aggregates in situ during the chain growth of the second block, which is also known as the polymerization-induced self-assembly.[16–19] Such a method offered an easy and practical approach to prepare the self-assembled structures at industrial scale. Wang et al.[16] prepared a variety of core−shell polymeric nanoparticle in situ in hexane by the growth of polystyrene (PS) block onto polybutadiene via living anionic polymerization, followed by the cross-linking of the formed PS core. Hashimoto and co-workers[17] investigated the self-assembly process of PI-PS during living anionic polymerization by in situ/real-time small-angle neutron scattering (SANS) in d_6-benzene. At high conversion, ordered structures, such as lamellar phase and hexagonally packed cylinder phase, were detected, and the disorder−order transition and the order−order transition could be observed.

Polymerization-induced self-assembly process is a dynamic process, where the polymerization (or chain growth) and the self-assembly are interdependent. On one hand, the self-assembly of the block copolymer is dependent on the total molecular weight and the block ratio, which are controlled by the polymerization process. Since both the block ratio and the molecular weight of the block copolymers increase continuously during the polymerization, the self-assembly of the block copolymer cannot reach its thermodynamic equilibrium until the polymerization terminates. Therefore, the aggregates are in the status of rearranging its structures throughout the polymerization process. On the other hand, depending on their locations upon forming aggregates, the "active" end groups of the polymer chain will lose or gain some activity during the self-assembly process. One extreme case is that all the "active" end groups are trapped inside the hard core of the micelle, which would dramatically slow down the polymerization rate. Therefore, the kinetics of polymerization is also subject to the self-assembly process.

To clarify the interrelationship between the polymerization process and the self-assembly process and, more importantly, to validate the method of polymerization induced self-assembly, we investigated the micellization of PEO-*b*-P(S-*alt*-MAn) during the growth of P(S-*alt*-MAn) block in dilute solution. The reversible addition−fragmentation chain transfer (RAFT)[20–22] method was employed for the polymerization. The RAFT method offers greater advantages over the classical living polymerization methods in preparing (co)polymers with low polydispersity from a large number of monomers under versatile conditions, and it is well-developed in dispersed systems.[23–27] During the polymerization-induced self-assembly process, the RAFT method is capable of preparing block copolymers with well-defined architecture and similar block length, which is crucial to obtain uniform micelles during polymerization.

The laser light scattering (LLS) technique is used to in situ monitor the micellization of PEO-*b*-P(S-*alt*-MAn) induced by the growth of P(S-*alt*-MAn) block in dilute solution. The time-resolved LLS has been successfully applied to determine the kinetics at the time scales from a few seconds to several hours. Two typical examples are the collapse of polymer chains[28–30] and the micellization of block copolymers,[31–35] both of which were triggered by the jump of either solvent quality or temperature. To minimize the errors induced by the fast kinetics during the LLS measurement, the rate of the polymerization-induced micellization was controlled to be slow, so that the sampling time was much shorter than the polymerization time as well as the micellization time.

Experimental Section

Materials. Polyethylene glycol monomethyl ether (mPEO, $\overline{M_n} \sim 5000$, $\overline{M_w}/\overline{M_n} \sim 1.05$) was purchased from Fluka Co. (Fluka, Switzerland). All the other reagents were purchased from Beijing Chemical Reagent Co. (Beijing, China). 2,2′-Azobis(isobutyronitrile) (AIBN) and MAn were purified twice by recrystallization in methanol and in CH_2Cl_2, respectively. Styrene (St) was washed in sequence with 10% aqueous NaOH and water, dried overnight with $MgSO_4$, and finally distilled over CaH_2 under reduced pressure. $CHCl_3$ was purified by refluxing with CaH_2. PEO macro-CTA (Scheme 1) was synthesized from mPEO according to a known procedure.[36]

* Corresponding authors: e-mail dliang@pku.edu.cn, Tel and Fax 86-10-62756170; e-mail zcli@pku.edu.cn, Tel 86-10-62757155; e-mail eqchen@pku.edu.cn, Tel 86-10-62753370.

10.1021/ma8005312 CCC: $40.75
Published on Web 06/05/2008

Scheme 1. Molecular Structure of PEO Macro-CTA

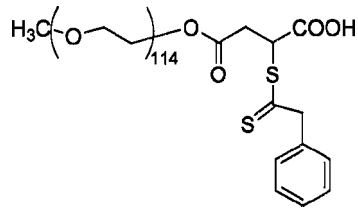

Polymerization. Typically, PEO macro-CTA (138 mg, 0.0253 mmol), MAn (199 mg, 2.03 mmol), styrene (211 mg, 2.02 mmol), and AIBN (4.0 mg, 0.0244 mmol) were mixed with 100 mL of $CHCl_3$. The solution was then filtrated into a dust-free cylindrical glass vial. O_2 was removed by purging pure N_2 for 5 min. The sample vial was then placed in a brass holder in the LLS setup with well-controlled temperature (±0.01 °C) at 55 °C. For polymerization at other concentrations, the amount of reagent was increased or decreased accordingly, wherein their molar ratios were kept constant. To determine the polymerization kinetics, a small portion (~0.5 mL) of the mixed solvent was taken out from the LLS vial at given time by a syringe under the protection of N_2. The sample was quickly quenched to room temperature, and the conversions of the monomers were determined by ^{1}H NMR. ^{1}H NMR spectra were obtained on a Varian-300 M spectrometer with $CDCl_3$ as the solvent and tetramethylsilane (TMS) as the internal reference for chemical shifts.

Light Scattering Measurements. Dynamic light scattering (DLS) and static light scattering (SLS) were conducted on a commercialized spectrometer from Brookhaven Instruments Corp. (Holtsville, NY). A solid-state laser polarized at the vertical direction (CNI Changchun GXL-III, 100mW, Changchun, China) operating at 532 nm was used as the light source.

For DLS, the intensity−intensity autocorrelation function $G^{(2)}(t,\theta)$ was measured in the self-beating mode. It is related to the normalized first order of electric field time correlation function $g^{(1)}(t,\theta)$ as

$$G^{(2)}(t,\theta) = \langle I(0,\theta)\, I(t,\theta)\rangle = A\left[1+\beta\left|g^{(1)}(t,\theta)\right|^2\right] \qquad (1)$$

where A is the measured baseline. The line width distribution $G(\Gamma)$ was analyzed with a Laplace inversion program, CONTIN, based on the following relation:

$$g^{(1)}(t,\theta) = \langle E(0,\theta)\, E^*(t,\theta)\rangle = \int_0^\infty G(\Gamma)\mathrm{e}^{-\Gamma t}\,\mathrm{d}\Gamma \qquad (2)$$

On the basis of the $\bar{\Gamma}$ of each peak given by the CONTIN program, the diffusion coefficient D can be calculated according to

$$\bar{\Gamma}/q^2 = D(1+k_\mathrm{d}C)[1+fR_\mathrm{g}{}^2q^2] \qquad (3)$$

where $q = 4\pi\mathrm{n}/\lambda\,\sin(\theta/2)$, with n, λ, C, R_g, k_d, and f being the solvent refractive index, the wavelength in vacuum, the concentration of the solution, the Z-average root-mean-square radius, the diffusion second virial coefficient, and a dimensionless constant, respectively. For a translational diffusion, the hydrodynamic radius R_h can be calculated using the Stokes−Einstein equation:

$$R_\mathrm{h} = \frac{k_\mathrm{B}T}{6\pi\eta D} \qquad (4)$$

where η is the viscosity of the solvent. The polydispersity value given by CONTIN is the quotient of the standard deviation and the mean peak position. Particularly, at the early stage of polymerization, where the excess scattered intensity was weak and the progress was very slow, the accumulation time for $G^{(2)}(\tau)$ is ca. 2 min; while at the later stages, where the increase in intensity was very fast, the accumulation time was reduced to as short as 10 s to avoid the undesired effects from polymerization. Although the accumulation time was relatively short, the quality of autocorrelation curves is still good enough to obtain reliable results, especially at 30°. During the later stage of polymerization, the scattered intensity is very high. Neutral density filters with known transmission ratio were used to attenuate the laser power, ensuring the linear response of the APD detector.

For SLS experiments, it is known that for a dilute solution measured at a relatively small angle θ the Rayleigh ratio $R_{vv}(q)$ is related to the weight-average molar mass M_w, the Z-average root-mean-square radius R_g, the second virial coefficient A_2, and scattering vector q as the following equation:

$$\frac{KC}{R_{vv}(q)} \approx \frac{1}{M_\mathrm{w}}\left(1+\frac{1}{3}R_\mathrm{g}{}^2q^2\right)+2A_2C \qquad (5)$$

where $K = 4\pi n^2(\mathrm{d}n/\mathrm{d}c)^2/(N_\mathrm{A}\lambda_0{}^4)$, with N_A and $(\mathrm{d}n/\mathrm{d}C)$ $b$eing the Avogadro constant and the specific refractive index increment of the solution, respectively. Since the scattered intensity of the sample keeps increasing during the polymerization, especially at the later stages, it is difficult to obtain the real-time angular dependence of the scattered intensity by using the conventional procedure. To correct for the time lag, we recorded the time dependence of the changes in the scattered intensity at each angle (30°, 45°, 60°, 75°, 90°). By using the standard cubic spline data interpolation method in MATLAB 6.5, we were able to obtain the angular dependence of the scattered intensity at a given time moment. With the conversion of the monomers, the viscosity and the refractive index of the solvent as well as the concentration (mg/mL) of the polymers were correspondingly changed. However, since the total amount of the monomer was less than 2.5 wt % of the solvent $CHCl_3$, the effect on the system parameters caused by monomer conversion was negligible.

Results and Discussion

In this work, we studied the polymerization-induced micellization of PEO-*b*-P(S-*alt*-MAn) in $CHCl_3$ using PEO macro-CTA via the RAFT method. The copolymerization of MAn and St by RAFT has been well studied.[37–40] It has been found that the copolymerization rate was much higher than that of the homopolymerization of St, and well-defined copolymers with predominant alternating structures could be obtained. $CHCl_3$ is a good solvent for PEO and a poor solvent for P(S-*alt*-MAn). Therefore, with the chain growth of the P(S-*alt*-MAn) block onto the PEO chain via RAFT, the micelles with P(S-*alt*-MAn) forming the core and PEO forming the corona are expected. The designed chemical composition of the resultant block copolymer is PEO_{114}-*b*-P(S-*alt*-$MAn)_{80}$ at 100% conversion. The polymerization was carried out at PEO macro-CTAs concentrations of 1.38−5.00 mg/mL and at high [PEO macro-CTA]/[AIBN] molar ratio to ensure the slow polymerization rate.

Figure 1 shows the evolution of the scattered intensity with time at different scattering angles. The concentration of PEO macro-CTAs is 1.38 mg/mL. The inset in Figure 1 shows the changes of the scattered intensity from 0 to 400 min. Clearly, the profile of the intensity in Figure 1 can be divided into three stages. In stage I (before 200 min), the scattered intensity was very weak and kept constant, indicating that the polymerization was in the induction period. Because the carbon-center radicals from AIBN decomposition reacted with oxygen at a rate much faster than that with the monomers, and the newly formed alkylperoxy radicals were very low in reactivity, the residual oxygen in the vial prevented the growth of the polymer chains. In stage II (from 200 to 370 min), a slightly increase in the scattered intensity was observed, suggesting that the O_2 in the vial had been depleted, and the polymer chain started to grow. Even though the scattered intensity in this stage was still weak, it exhibited a stronger angular dependence (inset in Figure 1). In stage III (after 370 min), the scattered intensity sharply increased, indicating the formation of micelles or aggregates.

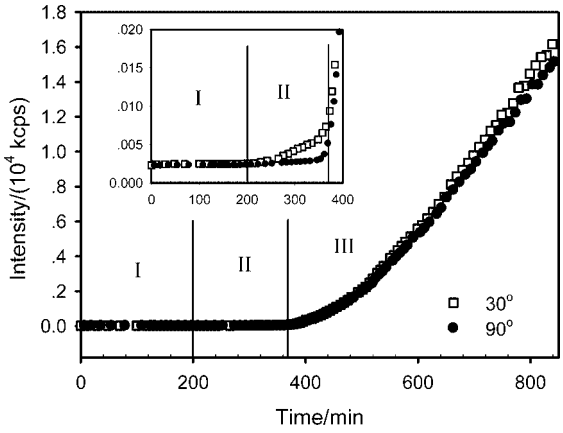

Figure 1. Time dependence of the scattered intensity at scattering angles of 30° and 90°. The concentration of PEO macro-CTA is 1.38 mg/mL. The inset shows the intensity change from 0 to 400 min.

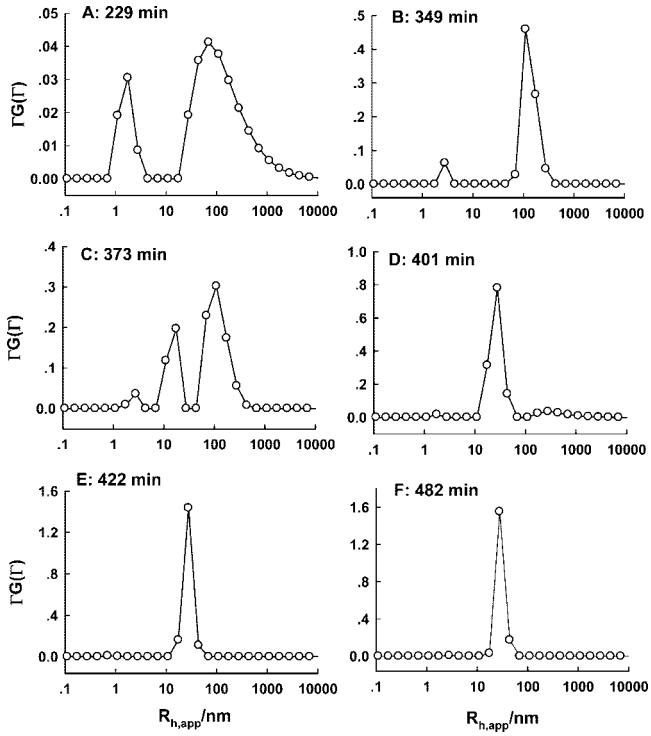

Figure 2. Distribution of hydrodynamic radius during polymerization at different time at 30°. The concentration of PEO macro-CTA is 1.38 mg/mL.

Interestingly, the stronger angular dependence observed in stage II was diminished.

Figure 2 shows the CONTIN analysis of the DLS results obtained at 30°. In stage I, because of the small size of PEO macro-CTA and the weak scattered intensity, the correlation curves accumulated for 2 min were too rough to yield reliable CONTIN results. While in stage II, a characteristic bimodal distribution, corresponding to the single polymer chains and a certain kind of aggregate, was observed (Figure 2A). With increasing reaction time, both the sizes of the single polymer chains and the aggregate were increased (Figure 2B), but the area ratio of the single polymer chains was reduced, indicating that more polymer chains formed aggregate with the growth of P(S-*alt*-MAn) block. Figure 2C shows that another aggregate, with the average $R_{h,app}$ value of ~20 nm, was formed in the early stage III. Actually, it was the very time that the scattered intensity started to sharply increase (Figure 1). After that, the original peaks corresponding to the single polymer chains or

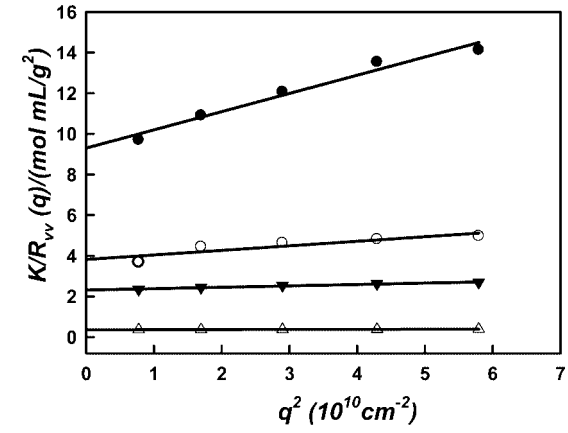

Figure 3. Typical angular dependence of $K/R_{vv}(q)$ at different reaction times: 380 min (●), 400 min (○), 420 min (▼), and 540 min (□), where K is a constant and the concentration of PEO macro-CTA is 1.38 mg/mL.

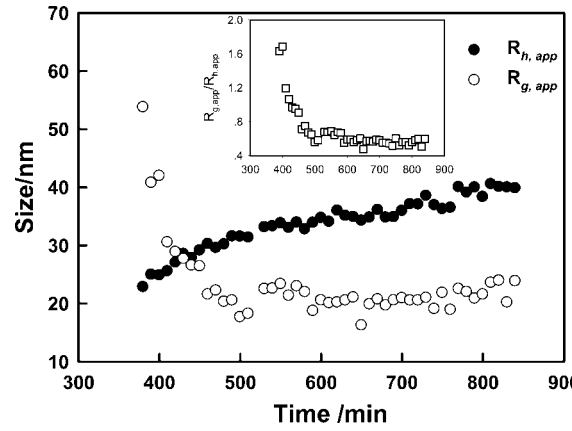

Figure 4. Time dependence of $R_{g,app}$ and $R_{h,app}$ in the polymerization-induced self-assembly process. The inset shows the changes in $R_{g,app}/R_{h,app}$. The concentration of PEO macro-CTA is 1.38 mg/mL.

aggregates were gradually diminished (Figure 2D). After ~420 min, only the newly formed aggregate with a narrow distribution remained in the system (Figure 2E), and its $R_{h,app}$ value slowly increased with the polymerization time.

As discussed above, both the scattered intensity and the size distributions exhibited strong changes in stage III. To clearly understand the polymerization-induced self-assembly process of PEO-*b*-P(S-*alt*-MAn) at this stage, we estimated the changes in $R_{g,app}$ by using the scattered intensity at different angles. Some representative curves are shown in Figure 3. Since there were more than one component in the system at the early polymerization period and it was difficult to differentiate their contribution to the scattered intensity, we only calculated the $R_{g,app}$ values at the time when one dominant component was remained in the system.

Figure 4 shows the time dependence of $R_{g,app}$ and $R_{h,app}$ of the major component shown in stage III. Clearly, $R_{h,app}$ was increased monotonically from 23 nm at 380 min to 40 nm at 840 min, while $R_{g,app}$ was decreased sharply from 53 nm to ~20 nm before 500 min and kept almost constant thereafter. Therefore, the $R_{g,app}/R_{h,app}$ ratio (inset in Figure 3) was correspondingly decreased from ~1.8 to ~0.5, indicating the conformational change from loose aggregate ($R_{g,app}/R_{h,app} > 1$) to hard spherical structures ($R_{g,app}/R_{h,app} < 0.775$).[41–43] It was now clear that the component remained in the system after 420 min was the micelles with P(S-*alt*-MAn) blocks forming the core and PEO blocks forming the shell.

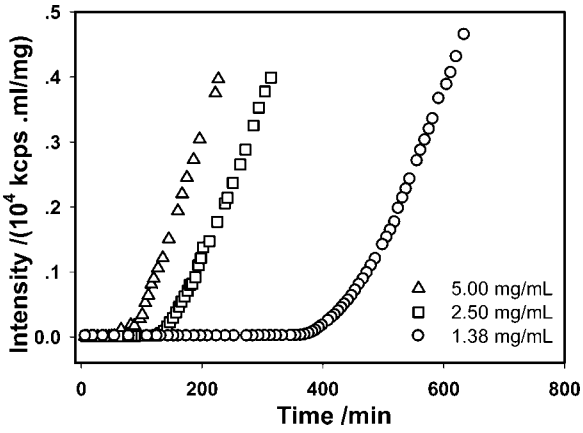

Figure 5. Time dependence of the scattering intensity of polymerization-induced self-assembly process at 90° at different PEO macro-CTA concentrations.

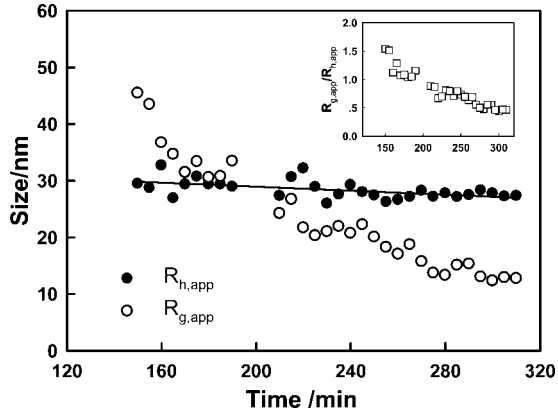

Figure 6. Time dependence of $R_{g,app}$ and $R_{h,app}$ during the polymerization-induced self-assembly process. The inset shows the changes in $R_{g,app}/R_{h,app}$. The concentration of PEO macro-CTA is 2.50 mg/mL.

Besides the core-forming block length, the concentration was another key parameter affecting the micelle formation. Figure 5 compares the scattered intensities with PEO macro-CTA at 1.38, 2.50, and 5.00 mg/mL. The intensity data in Figure 5 have been normalized by concentration for better comparison. Clearly, the polymerization-induced micellization of PEO-*b*-P(S-*alt*-MAn) at higher PEO macro-CTA concentrations exhibited a similar scattered intensity profile, which could also be divided into the three stages: the induction period, the formation of loose aggregate, and the formation of micelles. The major difference was that the polymerization carried out at higher concentration of PEO macro-CTA showed a shorter induction period and a faster increase in the scattered intensity.

Figure 6 shows the time dependence of $R_{g,app}$ and $R_{h,app}$ during the polymerization with 2.50 mg/mL PEO macro-CTA. The corresponding $R_{g,app}/R_{h,app}$ ratio is shown in the inset. Compared with the results in Figure 4, $R_{h,app}$ was ~29 nm and slightly decreased with time. In addition, no sharp decrease in $R_{g,app}$ was observed. The $R_{g,app}/R_{h,app}$ ratio shown in the inset was gradually decreased from ~1.5 to ~0.5, indicating a conformation transition from random coil to spherical structures.. When the concentration of PEO macro-CTAs was increased to 5.00 mg/mL, the $R_{h,app}$ in the later stages was reduced to ~23 nm (Figure 7) and was also slightly decreased with time. To confirm that PEO-*b*-P(S-*alt*-MAn) formed similar micellar structures at the PEO macro-CTA concentration ranging from 1.38 to 5.00 mg/mL, AFM experiments were conducted to compare the morphologies at the ending stages. Spherical structures were evidenced at PEO macro-CTA concentrations of 1.38 and 5.00

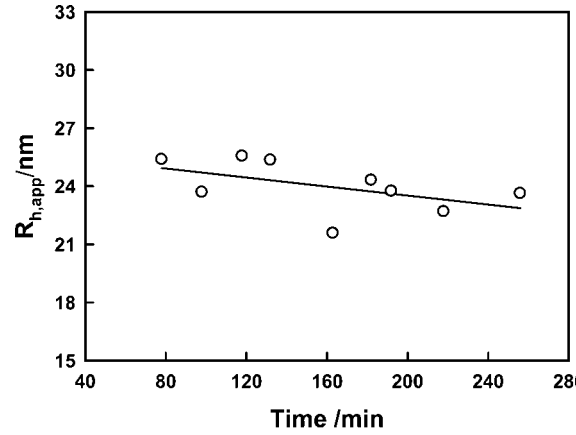

Figure 7. Time dependence of $R_{h,app}$ during the polymerization-induced micellization. The concentration of PEO macro-CTA is 5.00 mg/mL.

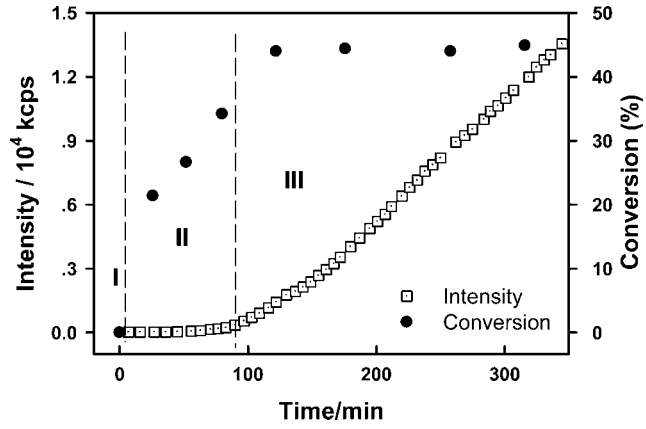

Figure 8. Comparison of the changes in the monomer conversion and the scattered intensity at 90° with increasing reaction time. The concentration of PEO macro-CTA is 5.00 mg/mL.

mg/mL, respectively (see the Supporting Information), agreeing well with the LLS results.

Figure 8 compares the rate of monomer conversion with the corresponding increase in the scattered intensity with reaction time. The concentration of PEO macro-CTA is 5.00 mg/mL. As shown in Figure 8, the scattered intensity and the rate of monomer conversion exhibited totally different behavior during the polymerization-induced micellization process. In stage II, the polymerization rate was very fast, even though the scattered intensity kept almost constant. While in stage III, the scattered intensity was dramatically increased due to the formation of micelles. The polymerization rate, on the other hand, was visually invariable. Actually, the monomer conversion was kept increasing, but at an extremely low rate, which was below the detection limit of the ^{1}H NMR. This indicated that the micellization had the tendency to retard the polymerization rate, which agreed with the findings by Zhang and Pan.[18] Figure 8 shows that, at the PEO macro-CTA concentration of 5.00 mg/mL, the maximum conversion rate of the monomers was ~45%, which corresponds to the P(S-*alt*-MAn) block length of 36.

The above results revealed several important features about the polymerization-induced micellization process in dilute solutions.

Critical Micelle Degree of Polymerization (CMDP). Since all the living chains were growing with similar rate by RAFT, it was rational to believe the existence of a CMDP value for the growing block during the polymerization. At the DP far below the CMDP, PEO-*b*-P(S-*alt*-MAn) chains could not self-assemble into micelles. They remained to be individual polymer

Scheme 2. Schematic Representation of the Polymerization-Induced Self-Assembly Process

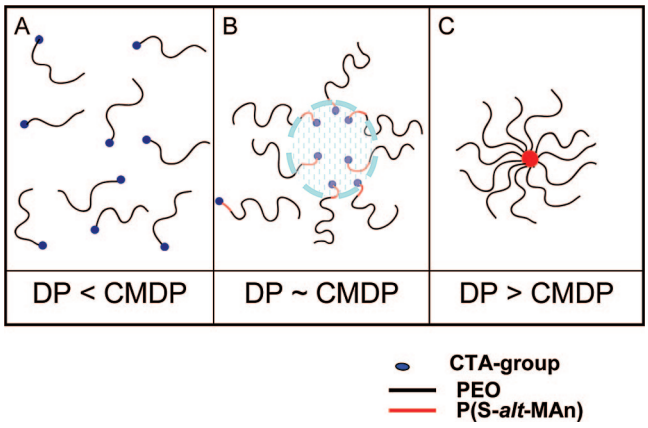

chains, similar to PEO macro-CTAs (Scheme 2A). With the DP increasing to a certain value, but still lower than CMDP, some of the PEO-*b*-P(S-*alt*-MAn) chains were associated together to form loose aggregates (Scheme 2B).The number and size of the loose aggregate were increased with increasing the DP of P(S-*alt*-MAn) block, which was demonstrated as the increase in the scattered intensity (the inset in Figure 1). Once the DP of P(S-*alt*-MAn) block exceeded the CMDP, the single polymer chains and the loose aggregate were gradually transformed into micelles, as shown in Scheme 2C. Therefore, the value of CMDP could be calculated from the transition point of loose aggregate to micelle. As shown in Figure 8, the CMDP value of P(S-*alt*-MAn) block at 5.0 mg/mL PEO macro-CTAs was corresponding to the monomer conversion at the borderline separating region II and III. It was calculated to be ~30 repeating units. It has been well-established in the literature that the core size and the aggregation number of the starlike micelle were $\propto N^{0.6-0.75}$ and $\propto N^{0.8-1.2}$, respectively, where N is the length of the core-forming block.[45,46] Therefore, with further increasing the DP of P(S-*alt*-MAn) block, both the aggregation number and the core size of the micelles were increased.

Concentration Effect. The CMDP value was concentration dependent. It was decreased with increasing PEO macro-CTA concentration; i.e., PEO-*b*-P(S-*alt*-MAn) chains formed micelles at earlier polymerization stage. Moreover, the increase in the concentration of PEO macro-CTAs also accelerated the polymerization rate. Both of these two effects resulted in a quick formation of micelles during the polymerization-induced micellization process, which was evidenced by the plots of the scattered intensities at different PEO macro-CTAs concentration (Figure 5). Another effect of concentration was tat it determined the size and morphology of the micelles formed during the polymerization. As shown in Figures 4 and 7, the $R_{h,app}$ values of the micelles formed at 1.38 mg/mL PEO macro-CTAs was increased from 23 to 40 nm with reaction time, while it was decreased from ~25 to ~23 nm at 5.00 mg/mL PEO macro-CTAs. The size of the micelle formed at 1.38 mg/mL PEO macro-CTAs at the ending stage was almost twice larger than that of at 5.00 mg/mL PEO macro-CTAs. Such a big difference in size could not be simply caused by the interactions between micelles, which was usually represented by the second viral coefficient (A_2 or k_d). Another interesting phenomenon was that, at 2.50 or 5.00 mg/mL PEO macro-CTAs, the size of the micelle was shrinking with time (Figures 6 and 7), but the scattered intensity was still sharply increasing (Figure 5).

Interrelationship between Polymerization and Micellization. The polymerization rate was highly dependent on the collisions of the "living" chains with monomers. At early polymerization stage, the PEO macro-CTA with shorter P(S-*alt*-MAn) block remained to be individual chains and was able to diffuse freely in the solution. Therefore, a steady polymerization (or monomer conversion) rate (Figure 8) was maintained. The formation of the loose aggregate exhibited a negligible effect on the polymerization rate in that the number of the aggregates was small, and they were in quick equilibrium with the single chains. However, the formation of micelles at the later stage dramatically decreased the polymerization rate (Figure 8). The solid-sphere-like micelles held the living chains together and "trapped" the transfer groups inside the core. Since the glass-transition temperature (T_g) of P(S-*alt*-MAn) block was much higher than 55 °C, the "residence time" of the polymer chains in the micelle was so long that almost no free single polymer chains could be observed in the system (Figure 2E,F). Without the free single chains, the polymerization rate was mainly determined by the diffusion of monomers into the core of the micelle, whose rate was much slower, mainly due to the barriers generated by the polymers chains in the micelle, than the free diffusion of the monomers. Moreover, P(S-*alt*-MAn) blocks were confined in a very limited space in the micellar core, which might also decrease the chain growth activity. All these effects, working together, strongly retarded the polymerization rate (Figure 8).

Even though the polymerization rate was dramatically slowed down after the formation of micelles, Figure 8 shows that the scattered intensity was still in the status of sharp increase in this stage. Based on eq 5, the scattered intensity was proportional to the square of the molecular weight and the square of the dn/dC value, or it was roughly proportional to the sixth power of the particle size. As mentioned above, the particle size was slowly decreasing with reaction time (except the $R_{h,app}$ in Figure 4); thus, its contribution to the increase in scattered intensity was negative or negligible. However, the molecular weight (or aggregation number) of the micelle was increasing almost linearly with the DP of P(S-*alt*-MAn) block.[45,46] Together with the shrinkage in size (at higher PEO macro-CTAs concentrations), an increase in the micelle density was deduced, which also resulted in a higher dn/dC value. Therefore, a slight growth of P(S-*alt*-MAn) block led to a sharp increase in the scattered intensity. It also explained the phenomenon that the scattered intensity increased with decreasing size, which was mentioned in the Concentration Effect section.

Kinetics of Micellization. During the polymerization process, the micelles were in a state of continuously adjusting the size and the aggregation number. The studies on the kinetics of micellization in the literature have revealed two basic kinetic processes: the incorporation of unimers into micelles without reaching the thermodynamic equilibrium and the reconstruction of micelles via the entry repulsion of unimers or fusion−fission of micelles to reach the equilibrium state.[31–35,47–49] The time scales of these processes were closely related with the polymer concentration, the addition of salt, and the jump of temperature or solvent quality. For Pluronic polymers, e.g. L64, the fast process was in the order of 0.01−1 ms, and the other process was in the order of 0.2−100 ms.[33,47] However, when the micellization of poly(α-methylstyrene)-*b*-poly(vinylphenethyl alcohol) in benzyl alcohol was studied by temperature jump, the time scales of the two processes were found to be 0.1−1 h and several tens of hours, respectively.[31,32] These results suggested that the micellization kinetics was also determined by the nature of the building blocks. During the polymerization-induced micellization process at fixed temperature, the micellization was induced mainly by the DP of the core-forming block. Once the DP of P(S-*alt*-MAn) block exceeded its CMDP, the unimers would incorporate into micelles, which was a relatively fast process. With further continuously increasing the

DP, the formed micelles were in the process of reconstructing the structures, and they never reach the equilibrium throughout the polymerization process, which was different from the micellization kinetic induced by the jump of temperature or solvent quality.

The kinetics of the micelle reconstruction during polymerization was determined by the difference between DP and CMDP. At lower polymer concentrations, the polymerization rate (or the increase in DP) was slow, and the micelles had longer time to make the adjustment on the structure and the aggregation number. Therefore, the system was in the state of thermodynamic equilibrium or at least was very close to it. While at higher polymer concentration, the increase in DP was very fast, and the micelles may not have enough time to make the adjustment. On the other hand, the enlargement in the difference between DP and CMDP also accelerated the rate of the micelle reconstruction, which resulted in a dynamic equilibrium between polymerization and micellization. Moreover, the micelles reconstructed in a fast rate may possess different structures compared with those obtained under the thermodynamic equilibrium. This was probably the reason that the size of the micelles followed a different trend with reaction time (referring to the Concentration Effect section) by varying the PEO macro-CTA concentrations from 1.38 to 5.00 mg/mL, as demonstrated in Figures 4, 6, and 7.

Our experiments not only revealed the features about the polymerization-induced micellization process but also indicated the importance of the strict control of the polymerization conditions. As shown in Figure 8, the increase in the scattered intensity at 5.00 mg/mL PEO macro-CTA was much slower than that at the same conditions but without taking samples from the system (Figure 5). Even though we were very cautious to not disturb the system when taking out the sample from the LLS vials, the accidental introduction of O_2 decreased the polymerization rate appreciably.

Conclusions

With proper control of the reaction conditions, polymerization-induced self-assembly showed great potential to prepare designed patterns at large scale. Our study on the micellization of PEO-*b*-P(S-*alt*-MAn) in $CHCl_3$ induced by the polymerization of P(S-*alt*-MAn) via RAFT has demonstrated that the polymerization and micellization were highly interdependent: the block copolymers formed micelles once the polymerization reached a certain degree; on the other hand, the polymerization rate was seriously retarded by the micelle formation. We also found that concentration was a crucial parameter in the polymerization-induced micellization process. Not only did it increase the rate of polymerization and micellization, it also affected profoundly on the micelles' structure, size, and aggregation number as well as the kinetics of micellization.

Acknowledgment. Financial support of this work from the National Nature Science Foundation of China (20474002, 20534010, 20504001) is gratefully acknowledged.

Supporting Information Available: Figures S1 and S2 showing morphologies of micelles at 5.00 and 1.38 mg/mL PEO-CTAs. This material is available free of charge via the Internet at http://pubs.acs.org.

References and Notes

(1) Bates, F. S.; Fredrickson, G. H. *Annu. Rev. Phys. Chem.* **1990**, *41*, 525–557.
(2) Matsen, M. W.; Bates, F. S. *Macromolecules* **1996**, *29*, 1091–1098.
(3) Halperin, A.; Tirrel, M.; Lodge, T. P. *Adv. Polym. Sci.* **1992**, *100*, 31.
(4) Hamley, I. W. *The Physics of Block Copolymers*; Oxford University Press: Oxford, 1998.
(5) Riess, G. *Prog. Polym. Sci.* **2003**, *28*, 1107–1170.
(6) Chu, B. Z. Z. In *Nonionic Surfactants. Polyoxyalkylene Block Copolymers*; Nace, V. N., Ed.; Marcel Dekker: New York, 1996; Vol. *60*.
(7) Cameron, N. S.; Corbierre, M. K.; Eisenberg, A. *Can. J. Chem.* **1999**, *77*, 1311–1326.
(8) Gohy, J. F. *Adv. Polym. Sci.* **2005**, *190*, 65–136.
(9) Bhargava, P.; Tu, Y. F.; Zheng, J. X.; Xiong, H. M.; Quirk, R. P.; Cheng, S. Z. D. *J. Am. Chem. Soc.* **2007**, *129*, 1113–1121.
(10) Zhang, G. Z.; Niu, A. Z.; Peng, S. F.; Jiang, M.; Tu, Y. F.; Li, M.; Wu, C. *Acc. Chem. Res.* **2001**, *34*, 249–256.
(11) Kabanov, A. V.; Batrakova, E. V.; Alakhov, V. Y. *J. Controlled Release* **2002**, *82*, 189–212.
(12) Gaucher, G.; Dufresne, M. H.; Sant, V. P.; Kang, N.; Maysinger, D.; Leroux, J. C. *J. Controlled Release* **2005**, *109*, 169–188.
(13) Forster, S.; Plantenberg, T. *Angew. Chem., Int. Ed.* **2002**, *41*, 689–714.
(14) Gates, B. D.; Xu, Q. B.; Love, J. C.; Wolfe, D. B.; Whitesides, G. M. *Annu. Rev. Mater. Res.* **2004**, *34*, 339–372.
(15) Gates, B. D.; Xu, Q. B.; Stewart, M.; Ryan, D.; Willson, C. G.; Whitesides, G. M. *Chem. Rev.* **2005**, *105*, 1171–1196.
(16) Wang, X. R.; Hall, J. E.; Warren, S.; Krom, J.; Magistrelli, J. M.; Rackaitis, M.; Bohm, G. G. A. *Macromolecules* **2007**, *40*, 499–508.
(17) Yamauchi, K.; Hasegawa, H.; Hashimoto, T.; Tanaka, H.; Motokawa, R.; Koizumi, S. *Macromolecules* **2006**, *39*, 4531–4539.
(18) Zheng, G. H.; Pan, C. Y. *Macromolecules* **2006**, *39*, 95–102.
(19) Wan, W. M.; Pan, C. Y. *Macromolecules* **2007**, *40*, 8897–8905.
(20) Chiefari, J.; Chong, Y. K.; Ercole, F.; Krstina, J.; Jeffery, J.; Le, T. P. T.; Mayadunne, R. T. A.; Meijs, G. F.; Moad, C. L.; Moad, G.; Rizzardo, E.; Thang, S. H. *Macromolecules* **1998**, *31*, 5559–5562.
(21) Moad, G.; Chiefari, J.; Chong, Y. K.; Krstina, J.; Mayadunne, R. T. A.; Postma, A.; Rizzardo, E.; Thang, S. H. *Polym. Int.* **2000**, *49*, 993–1001.
(22) Lowe, A. B.; McCormick, C. L. *Prog. Polym. Sci.* **2007**, *32*, 283–351.
(23) Bussels, R.; Bergman-Gottgens, C.; Meuldijk, J.; Koning, C. *Macromolecules* **2004**, *37*, 9299–9301.
(24) Shim, S. E.; Lee, H.; Choe, S. *Macromolecules* **2004**, *37*, 5565–5571.
(25) Ferguson, C. J.; Hughes, R. J.; Nguyen, D.; Pham, B. T. T.; Gilbert, R. G.; Serelis, A. K.; Such, C. H.; Hawkett, B. S. *Macromolecules* **2005**, *38*, 2191–2204.
(26) Vosloo, J. J.; De Wet-Roos, D.; Tonge, M. P.; Sanderson, R. D. *Macromolecules* **2002**, *35*, 4894–4902.
(27) Lansalot, M.; Davis, T. P.; Heuts, J. P. A. *Macromolecules* **2002**, *35*, 7582–7591.
(28) Chu, B.; Ying, Q. C.; Grosberg, A. Y. *Macromolecules* **1995**, *28*, 180–189.
(29) Wang, X. H.; Qiu, X. P.; Wu, C. *Macromolecules* **1998**, *31*, 2972–2976.
(30) Wu, C.; Wang, X. H. *Phys. Rev. Lett.* **1998**, *80*, 4092–4094.
(31) Honda, C.; Hasegawa, Y.; Hirunuma, R.; Nose, T. *Macromolecules* **1994**, *27*, 7660–7668.
(32) Honda, C.; Abe, Y.; Nose, T. *Macromolecules* **1996**, *29*, 6778–6785.
(33) Kositza, M. J.; Bohne, C.; Alexandridis, P.; Hatton, T. A.; Holzwarth, J. F. *Macromolecules* **1999**, *32*, 5539–5551.
(34) Kositza, M. J.; Rees, G. D.; Holzwarth, A.; Holzwarth, J. F. *Langmuir* **2000**, *16*, 9035–9041.
(35) Ye, X. D.; Lu, Y. J.; Liu, S. L.; Zhang, G. Z.; Wu, C. *Langmuir* **2007**, *23*, 10366–10371.
(36) Hong, C. Y.; You, Y. Z.; Pan, C. Y. *J. Polym. Sci., Part A: Polym. Chem.* **2004**, *42*, 4873–4881.
(37) De Brouwer, H.; Schellekens, M. A. J.; Klumperman, B.; Monteiro, M. J.; German, A. L. *J. Polym. Sci., Part A: Polym. Chem.* **2000**, *38*, 3596–3603.
(38) Park, E. S.; Kim, M. N.; Lee, I. M.; Lee, H. S.; Yoon, J. S. *J. Polym. Sci., Part A: Polym. Chem.* **2000**, *38*, 2239–2244.
(39) Zhu, M. Q.; Wei, L. H.; Li, M.; Jiang, L.; Du, F. S.; Li, Z. C.; Li, F. M. *Chem. Commun.* **2001**, 365–366.
(40) Harrisson, S.; Wooley, K. L. *Chem. Commun.* **2005**, 3259–3261.
(41) Qiu, X. P.; Wu, C. *Macromolecules* **1997**, *30*, 7921–7926.
(42) Chen, H. W.; Zhang, Q. J.; Li, J. F.; Ding, Y. W.; Zhang, G. Z.; Wu, C. *Macromolecules* **2005**, *38*, 8045–8050.
(43) Burchard, W. *Adv. Polym. Sci.* **1983**, *48*, 1–124.
(44) Forster, S.; Zisenis, M.; Wenz, E.; Antonietti, M. *J. Chem. Phys.* **1996**, *104*, 9956–9970.
(45) Halperin, A. *Macromolecules* **1987**, *20*, 2943–2946.
(46) Nagarajan, R.; Ganesh, K. *J. Chem. Phys.* **1989**, *90*, 5843–5856.
(47) Michels, B.; Waton, G.; Zana, R. *Langmuir* **1997**, *13*, 3111–3118.
(48) Dormidontova, E. E. *Macromolecules* **1999**, *32*, 7630–7644.
(49) Waton, G.; Michels, B.; Zana, R. *Macromolecules* **2001**, *34*, 907–910.

MA8005312